Discover Sustainability

RESEARCH Open Access

SDS stabilized CuO nanoparticles as dual functional agents for antifungal and photocatalytic applications

Iqra Ramzan[1], Babar Shahzad Khan[1], Sardar Sikandar Hayat[2], Sajjad Hyder[3], Nimra Asmat[1], Bismmah Shakir[1], Adnan Saeed[1], Mahwish Bashir[1], . Iqra[4], Zarrin Fatima Rizvi[3] and Mudassir Iqbal[4*]

*Correspondence:
Mudassir Iqbal
mudassir.iqbal@slu.se
[1]Department of Physics, GC Women University Sialkot, Sialkot 51310, Pakistan
[2]Department of Physics, International Islamic University Islamabad, Islamabad 44000, Pakistan
[3]Department of Botany, GC Women University Sialkot, Sialkot 51310, Pakistan
[4]Department of Plant Protection Biology, Swedish University of Agricultural Sciences, 23422 Lomma, Sweden

Abstract
Copper oxide nanoparticles (CuO NPs) are emerging as promising multifunctional agents for agriculture and environmental remediation. Here, we report the laboratory-scale synthesis of sodium dodecyl sulfate (SDS)-stabilized CuO NPs via a co-precipitation method, optimising NaOH concentrations to adjust particle characteristics. X-ray diffraction (XRD) confirmed a crystalline monoclinic structure, while scanning electron microscopy (SEM) revealed well-dispersed, spherical nanoparticles ranging from ~27 to 95 ± 5 nm. SDS stabilization effectively prevented agglomeration and enhanced nanoparticle dispersibility. UV–Vis spectroscopy revealed optical band gaps ranging from 4.16 to 4.52 eV, values higher than typical bulk CuO likely due to nanoscale effects and SDS interactions. The nanoparticles demonstrated approximately 62.2% and 66.4% mycelial growth inhibition against *Pythium myriotylum* and *Phytophthora capsici*, respectively, under *in vitro* conditions. Additionally, the SDS-CuO NPs achieved up to 94% degradation of methylene blue under UV light after 90 min, indicating effective photocatalytic activity in model dye systems. These findings suggest the potential of SDS-CuO NPs for dual applications, though further work is needed to evaluate reusability, environmental impact, and field-level performance.

Keywords CuO NPs, SDS stabilization, Antifungal activity, Photocatalysis, Reactive oxygen species (ROS), Wastewater remediation

1 Introduction

Chili pepper (*Capsicum annuum* L.), a widely cultivated member of the Solanaceae family, is an essential crop in tropical and subtropical regions and a staple in many global cuisines [1]. However, its production is threatened by several plant pathogens that severely impact yield and quality [2]. Among these, *Pythium myriotylum* and *Phytophthora capsici* are particularly damaging, causing damping-off and root rot diseases, especially during early plant development [3, 4]. While *P. myriotylum* typically affects

seedlings at the cotyledonous stage, *P. capsici* can cause complete crop failure under favourable conditions [2, 5].

Conventional control methods primarily rely on chemical fungicides. Although these treatments can be effective, they pose serious environmental and health risks, are expensive, and contribute to the emergence of resistant pathogen strains. As alternatives, biological control strategies using microbial antagonists have been explored. These approaches involve mechanisms such as hyperparasitism, antibiosis, and predation [6–8], but their effectiveness is often limited by high specificity, variable environmental performance, and poor adaptability to different soil and crop conditions [9, 10]. This highlights the urgent need for safer, more reliable, and environmentally compatible alternatives to conventional chemical fungicides [11, 12], while recognising that their broader ecological impacts must be carefully evaluated. In parallel, environmental pollution caused by industrial dyes presents another major challenge. Methylene blue (MB), widely used in textiles, cosmetics, and pharmaceuticals, is highly persistent in wastewater due to its complex aromatic structure. Its degradation byproducts are often toxic and carcinogenic, posing serious ecological threats [13, 14]. Therefore, effective and eco-friendly methods for wastewater treatment are also critically needed.

Engineered nanomaterials have recently emerged as promising tools for addressing both agricultural and environmental challenges due to their enhanced surface reactivity, multifunctionality, and tunable physicochemical properties. Given the global demand for integrated, resource-efficient solutions, developing multifunctional nanomaterials that can simultaneously manage plant pathogens and environmental pollutants offers a strategic advantage for environmentally compatible and application-oriented solutions. Among these, metal oxide nanoparticles are particularly attractive for their broad-spectrum antimicrobial activity and catalytic potential [15, 16]. Copper oxide (CuO), a p-type semiconductor, stands out for its low cost, ease of synthesis, and ability to generate reactive oxygen species (ROS), which contribute to both microbial inactivation and degradation of organic pollutants [17–19]. The antimicrobial efficacy of copper oxide nanoparticles (CuO NPs) is attributed to mechanisms such as membrane disruption, intracellular ROS generation, and interference with metabolic pathways [20, 21]. Additionally, CuO exhibits strong photocatalytic activity under UV and visible light due to efficient charge separation and redox potential, making it a viable candidate for dye degradation and wastewater treatment applications [22, 23]. Recent studies have demonstrated CuO's effectiveness against plant pathogens and in environmental remediation, with promising outcomes in terms of both inhibition efficiency and catalytic degradation rates [24]. These multifunctional properties position CuO as a dual-action material suitable for integrated pest and pollution management systems.

The size, shape, and stability of CuO NPs play important roles in their functionality [25, 26], and various synthesis approaches have been developed, including hydrothermal [27], electrochemical [18], biogenic [28], chemical precipitation [29], and sol-gel methods [30]. CuO NPs produced via these methods have shown strong antifungal activity against plant pathogens [31, 32]. For example, Thakur et al. synthesized CuO NPs using *Asparagus adscendens* extracts and reported significant antibacterial effects [32], while Sawake et al. demonstrated the antifungal potential of biogenic CuO NPs against *Phytophthora parasitica* [28]. Similarly, cuprous oxide NPs have been reported to control *Fusarium solani* and reduce root rot in cucumber [33].

Among the available synthesis techniques, chemical precipitation stands out for its simplicity, scalability, and cost-effectiveness. The addition of surfactants such as polyvinylpyrrolidone (PVP) [34, 35], sodium dodecyl sulphate (SDS) [36], cetyl trimethyl ammonium bromide (CTAB) [37], ethylene glycol [38], sodium polyacrylate [39], and polyethylene glycol (PEG) [40, 41] plays a critical role in controlling nanoparticle morphology and stability. In this study, SDS was chosen as the stabilizing agent due to its unique combination of functional advantages. As a low-cost, widely available anionic surfactant, SDS provides strong electrostatic stabilization that minimizes nanoparticle agglomeration during synthesis [42]. In contrast to non-ionic (PVP) or cationic (CTAB) alternatives, SDS also possesses inherent microbicidal properties, potentially enhancing the antifungal efficacy of CuO NPs. Additionally, its widespread use in biological systems and documented biodegradability [43] make it an environmentally compatible choice, aligning with the sustainability goals of agricultural and wastewater treatment applications.

Although CuO NPs have been widely studied for either photocatalytic or antifungal applications, integrated studies demonstrating both functionalities within a single nanomaterial system remain limited. In particular, the dual use of SDS-stabilized CuO NPs, which combine improved colloidal stability, microbicidal synergy, and photocatalytic performance, has not been systematically explored. Prior work has addressed these roles separately, but comprehensive evaluation against aggressive phytopathogens such as *P. myriotylum* and *P. capsici* is scarce, and few studies link such biological targets with concurrent environmental remediation goals.

To address this gap, we synthesized SDS-stabilized CuO NPs via a simple chemical precipitation method and characterized their structural, morphological, and optical properties. Their antifungal efficacy and photocatalytic performance were evaluated using biologically and environmentally relevant test systems. This study aims to advance multifunctional nanomaterials by demonstrating a cost-effective, dual-action platform for both plant disease control and wastewater treatment.

2 Materials and methods

2.1 Synthesis of CuO NPs

CuO NPs were synthesized using a simple aqueous precipitation method [44; Fig. 1]. Copper chloride ($CuCl_2$, Sigma-Aldrich, 99%) and copper nitrate ($Cu(NO_3)_2{\cdot}3\ H_2O$, Sigma-Aldrich, ~99%) were used as precursor salts. A combination of these two copper salts was chosen to create a mixed anion environment, which influences solubility, ion release rates, and nucleation kinetics, ultimately aiding in uniform particle formation and dispersion. NaOH (Merck, ~99%) served as an alkaline reagent. SDS (Sigma-Aldrich, ~99%) was included as a surfactant to aid nanoparticle stabilization. All chemicals were of analytical grade and used without further purification.

Initially, 50 mL of 1M aqueous solutions of $Cu(NO_3)_2{\cdot}3\ H_2O$, $CuCl_2$, and SDS were prepared separately. NaOH solutions of 1 M, 3 M, and 5 M were also prepared in distilled water. The precursor ($Cu(NO_3)_2$ and $CuCl_2$) and surfactant (SDS) solutions were combined in a round-bottom flask and stirred continuously for 20 min to ensure homogeneity. Subsequently, NaOH solution was added dropwise under continuous stirring while maintaining a constant temperature of 60 °C. The reaction was allowed to proceed for 2 h with continuous stirring, during which the addition of NaOH raised the pH above

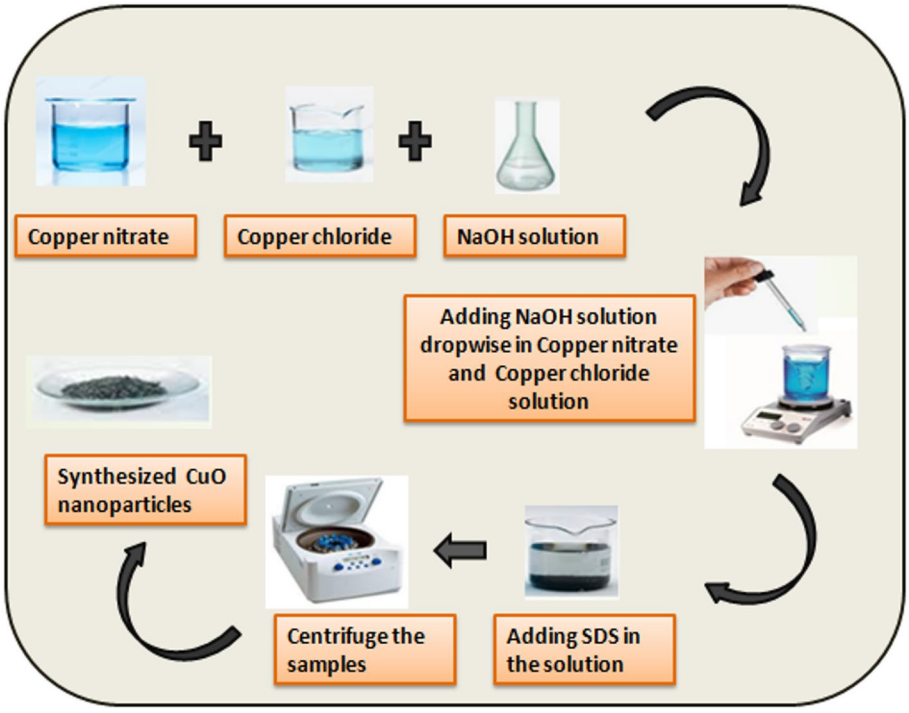

Fig. 1 Schematic illustration of the synthesis procedure for SDS-stabilized copper oxide nanoparticles (CuO NPs). The process involves the co-precipitation of copper nitrate and copper chloride with sodium hydroxide (NaOH), followed by the addition of sodium dodecyl sulphate (SDS) for nanoparticle stabilization, centrifugation, and collection of the final CuO NPs product

10 to promote CuO precipitation. After synthesis, the precipitate was washed repeatedly with distilled water until the wash solution reached neutral pH (~7). The total reaction volume was maintained at approximately 150 mL.

The resulting precipitates were collected by centrifugation at 3000 rpm, thoroughly washed with double-distilled water to remove impurities, and subsequently dried at 50 °C. The precipitate initially appeared light blue and gradually turned dark brownish black upon drying, indicating the formation of CuO. Three different samples of CuO NPs were synthesized by varying the molar ratio of NaOH relative to the fixed amounts of copper precursors and SDS. Sample 1 was prepared using $Cu(NO_3)_2{\cdot}3\ H_2O$, $CuCl_2$, SDS, and NaOH in a molar ratio of 1:1:1:1. Sample 2 followed the same procedure but with a 1:1:1:3 molar ratio, while Sample 3 used a 1:1:1:5 ratio. This variation in NaOH molar equivalents was aimed at studying its effect on the structural and morphological properties of the synthesized CuO NPs. These ratios were selected based on preliminary screening experiments to explore how varying alkalinity influences the size, crystallinity, and functional behaviour of the resulting CuO NPs. SDS played a critical role during the co-precipitation process. Its anionic sulphate groups adsorb onto the surface of growing CuO NPs, introducing electrostatic repulsion that inhibits particle agglomeration [36, 42]. This stabilization mechanism facilitates more uniform crystal growth and contributes to controlling nanoparticle size and dispersion, as later confirmed by scanning electron microscopy (SEM) and X-ray diffraction (XRD) analyses.

2.2 Characterizations of CuO NPs

The successful formation of SDS-capped CuO NPs was confirmed through various characterization techniques. XRD analysis was carried out using a Bruker D8 Advance X-ray diffractometer (Germany) with Cu-Kα radiation (λ = 1.5405 Å) operated at 40 kV and 30 mA to determine the crystalline structure of the nanoparticles. The scan was performed over a 2θ range of 10°–80° with a step size of 0.02° and scan speed of 1°/min. The morphology and elemental composition of the synthesized CuO NPs were examined using SEM coupled with energy-dispersive X-ray spectroscopy (EDX) (JEOL JSM-7600 F, Japan) at a working voltage of 10 kV. Samples were sputter-coated with a thin gold layer (~ 10 nm) prior to imaging to enhance conductivity and image resolution. Optical properties were investigated using UV-visible spectroscopy (SPECORD 210 Plus, Germany), where nanoparticles were ultrasonically dispersed in deionized water for 10 min and scanned over a wavelength range of 200–800 nm. The functional groups and molecular interactions were analysed through Fourier-transform infrared spectroscopy (FTIR) (PerkinElmer 1650, USA) using the KBr pellet method, recorded over a spectral range of 400–4000 cm^{-1} with a resolution of 4 cm^{-1} and 32 scans per sample.

2.3 Photocatalytic properties

The photocatalytic activity (PCA) of SDS-assisted CuO NPs was evaluated by monitoring the degradation of methylene blue (MB) under UV light (λ = 365 nm) irradiation using a 300 W mercury vapor lamp positioned 15 cm above the reaction mixture. For this analysis, 30 mg of synthesized SDS/CuO (1:1:1) nanoparticles was dispersed in 50 mL of aqueous MB solution. Prior to illumination, the suspension was stirred in the dark for 30 min to establish adsorption–desorption equilibrium. The mixture was then continuously stirred under UV exposure for 90 min to ensure uniform dispersion and reaction of the photocatalyst.

To assess the dye degradation, UV-visible (UV-vis) spectra were recorded at regular intervals of 5 min. For each measurement, a 3 mL aliquot was withdrawn from the reaction flask and centrifuged to separate the residual photocatalyst particles. The clear supernatant was then analysed using a UV-vis spectrophotometer. The degradation rate of MB was calculated using the following equation [45].

$$Degredation\ Rate\ (\%) = \frac{A_o - A_t}{A_o} \times 100\%$$

where, A_o is the initial concentration of dye and A_t is the concentration of dye after treatment at different time intervals.

2.4 Fungal species

The antifungal activity of SDS/CuO NPs was evaluated against two previously reported virulent fungal strains: *P. myriotylum* (accession no. MF143429) and *P. capsici* (accession no. MF322868), both known causal agents of damping-off disease in chili crops [3, 4, 46]. The fungal isolates were obtained from the Department of Botany, Government College Women University Sialkot (GCWUS), Pakistan (https://gcwus.edu.pk/faculties/faculty-of-natural-science/botany/). These fungal species were cultured on potato dextrose agar (PDA) medium (HCM050, HKM, China) and incubated at 25 ± 2 °C under

dark conditions to ensure optimal growth and virulence. Subculturing was performed every 7 days to maintain viability and pathogenicity.

2.5 Antifungal assay of CuO NPs

The antifungal activity of SDS-assisted CuO NPs was assessed *in vitro* against *P. myriotylum* and *P. capsici* following the method as described previously [31]. The nanoparticles were tested at three different concentrations: 100 ppm, 200 ppm, and 300 ppm. Freshly prepared PDA plates were inoculated with seven-day-old cultures of *P. myriotylum* and *P. capsici* by placing fungal discs on one side of the Petri dish. On the opposite side, sterilized paper discs loaded with 10 µL of CuO NPs suspensions at the respective concentrations were placed. Control plates contained only fungal cultures without CuO NPs treatment. All treatments were performed in triplicate ($n = 3$). Colony diameter was measured in two perpendicular directions, and the average was used to calculate growth inhibition to minimize measurement bias. All plates were incubated at 25 ± 2 °C for 5 days, and fungal growth inhibition was recorded using the following method.

$$\%\ Mycelial\ Growth\ Inhibition = \frac{C - T}{C} \times 100$$

C = Mycelial growth in control; T = Mycelial growth in treatment.

2.6 Statistical analysis

The *in vitro* antagonism assay data were analysed using ANOVA in Statistix (ver. 8.1). Pairwise comparisons were conducted using Fisher's least significant difference (LSD) at 95% significance level.

3 Results

3.1 Structural analysis of SDS-coated CuO NPs

The structural characteristics of SDS/CuO NPs were analysed using X-ray diffraction (XRD; Fig. 2). The XRD patterns confirm the formation of a single-phase monoclinic CuO structure across all samples. The diffraction peaks observed at 2θ = 32.70°, 35.67°, 38.95°, 49.01°, 53.56°, 58.53°, 61.72°, 65.95°, and 68.38° correspond to the (110), ($\bar{1}$11), (111), ($\bar{2}$02), (020), (202), ($\bar{1}$13), (022), and (220) crystal planes, respectively, which are consistent with the standard reference data (JCPDS card No. 65-2309) [47].

As depicted in Fig. 2, the NaOH concentration significantly influences the crystallinity of CuO NPs. Importantly, at a volumetric ratio of 1:1:5, the intensity of the diffraction peaks increases, indicating improved crystallinity, and additional peaks emerge (Fig. 2c). Moreover, no impurity phases such as Cu_2O, Cu, or $Cu(OH)_2$ were detected, confirming the high phase purity of the synthesized nanoparticles [48]. The average crystallite size of the CuO NPs was estimated using the Scherrer equation [49].

$$S = \frac{0.9\lambda}{\beta\, Cos\theta}$$

where β represents the full width at half maximum (FWHM), S is the crystallite size, λ is the X-ray wavelength (1.54056 Å for Cu-Kα radiation), and θ is the Bragg angle. Broadening of XRD peaks was observed, suggesting nanoscale crystallite size and potential micro strain within the crystal lattice. The estimated crystallite size of CuO NPs ranges

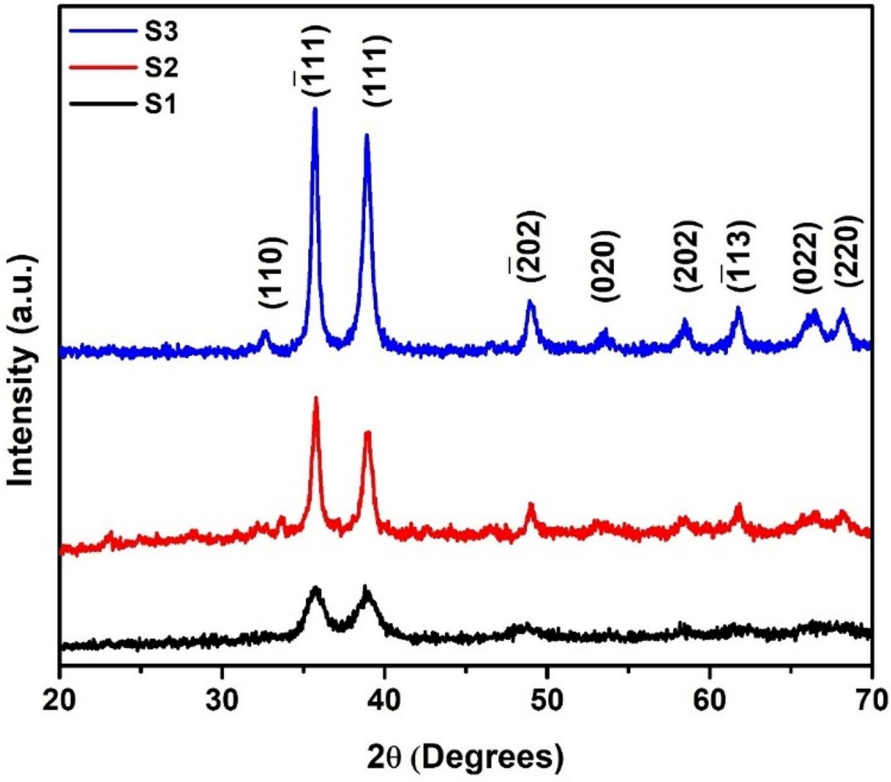

Fig. 2 X-ray diffraction (XRD) patterns of SDS/CuO nanoparticles (CuO NPs) synthesized at different molar ratios of precursor: surfactant: NaOH. **a** Molar ratio 1:1:1, **b** Molar ratio 1:1:3, and **c** Molar ratio 1:1:5. The diffraction peaks indicate the formation of monoclinic CuO phase, with variations in peak intensity and crystallinity observed with changes in the NaOH concentration

from 19 to 80 nm. This broad size distribution reflects variation among the three samples synthesized at different NaOH concentrations, with larger crystallites forming at higher alkalinity. Since SDS acts solely as a stabilizing agent and does not form a crystalline phase, only the CuO component was analysed for crystallite size. Furthermore, the average nanoparticle size calculated using the Scherrer equation aligns well with the SEM analysis, confirming the consistency of the structural and morphological results.

3.2 SEM analysis

The morphology and size distribution of the synthesized CuO NPs were examined using SEM (Fig. 3). The analysis revealed that the nanoparticles were well-dispersed and exhibited a spherical shape, with sizes ranging from ~ 27 to 95 ± 5 nm. The effect of NaOH concentration on nanoparticle size was evident. At lower NaOH concentrations (1:1:1 and 1:1:3 volume ratios), the CuO NPs appeared smaller but showed noticeable agglomeration (Fig. 3a, c). However, as the NaOH concentration increased (1:1:5 ratio), the average nanoparticle diameter grew to ~ 95 ± 5 nm, and a qualitative improvement in particle separation was observed, suggesting reduced agglomeration (Fig. 3e). This trend may be attributed to improved SDS-mediated stabilization at higher pH, although we recognize that agglomeration can also be influenced by drying conditions, ionic strength, and surface interactions. The synthesis procedure was repeated under identical conditions for each molar ratio, and SEM analysis of replicate batches confirmed consistent morphology and particle dispersion, indicating good reproducibility of the method.

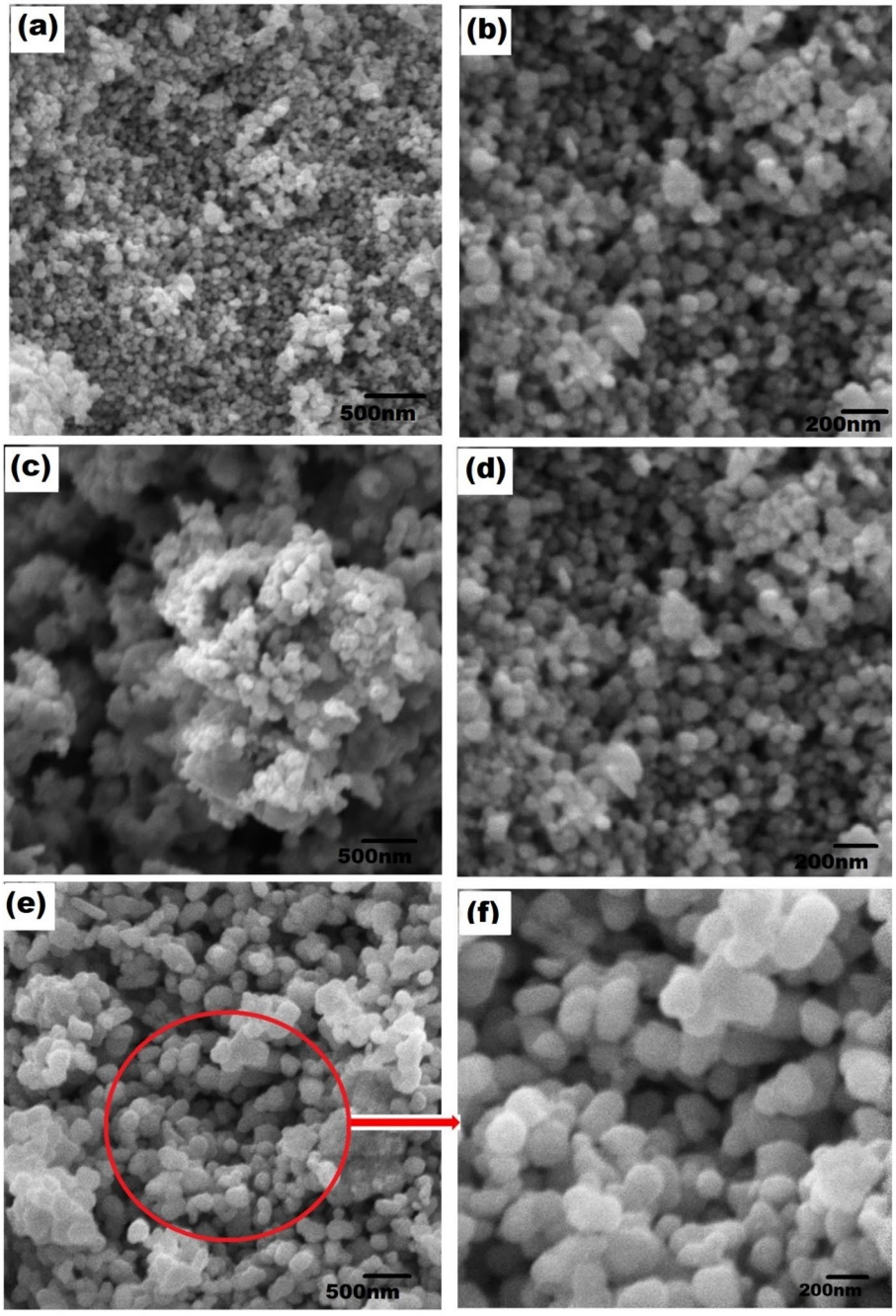

Fig. 3 Scanning electron microscopy (SEM) images of SDS-mediated CuO nanoparticles (CuO NPs) synthesized at different molar ratios of precursor: surfactant: NaOH. **a** Molar ratio 1:1:1, **b** Magnified view of the 1:1:1 sample showing particle size and morphology, **c** Molar ratio 1:1:3, **d** Magnified view of the 1:1:3 sample highlighting particle dispersion, **e** Molar ratio 1:1:5, and **f** Magnified view of the 1:1:5 sample showing reduced agglomeration

3.3 EDX spectroscopy analysis

EDX spectroscopy was performed to confirm the presence of CuO NPs and analyse the elemental composition of the synthesized samples. EDX analysis was performed on a representative CuO sample (sample 2). Although SDS was used as a capping agent, no sulphur peaks were detected, likely due to its low surface concentration and the limited sensitivity of EDX to light organic elements. The EDX spectra clearly indicated

the presence of copper (Cu) and oxygen (O) in the examined sample, with no detectable impurity elements, confirming the high purity of the synthesized CuO NPs (Fig. 4). The atomic composition of Cu and O, was determined to be Cu–75.64% and O–24.36%. Although this deviates from the ideal 1:1 stoichiometry of CuO, such discrepancies are common in EDX analysis due to its limited sensitivity to light elements like oxygen, which can result in underestimation. Other contributing factors may include surface oxidation states, beam-sample interactions, or slight compositional inhomogeneity. Additionally, sample preparation and electron beam exposure may contribute to the apparent imbalance. However, phase purity confirmed by XRD supports the successful formation of monoclinic CuO.

3.4 UV-vis absorption spectroscopy

UV-vis absorption spectroscopy was used to investigate the optical properties of the synthesized CuO NPs. Figure 5a presents the UV-vis absorption spectra alongside the EDX data of the SDS/CuO NPs. The absorption spectra revealed three prominent peaks at wavelengths 298 nm, 282 nm, and 274 nm, indicating the characteristic optical behaviour of the CuO NPs.

The band gap of the nanoparticles, calculated from the UV-vis data, was found to range between 4.16 eV and 4.52 eV. These values are higher than typical bulk CuO band gaps (~1.2 to 2.1 eV), likely due to quantum confinement effects associated with the small particle size. Surface interactions with the SDS stabilizer and the assumption of a direct electronic transition in the Tauc analysis may also contribute to the observed shift. The

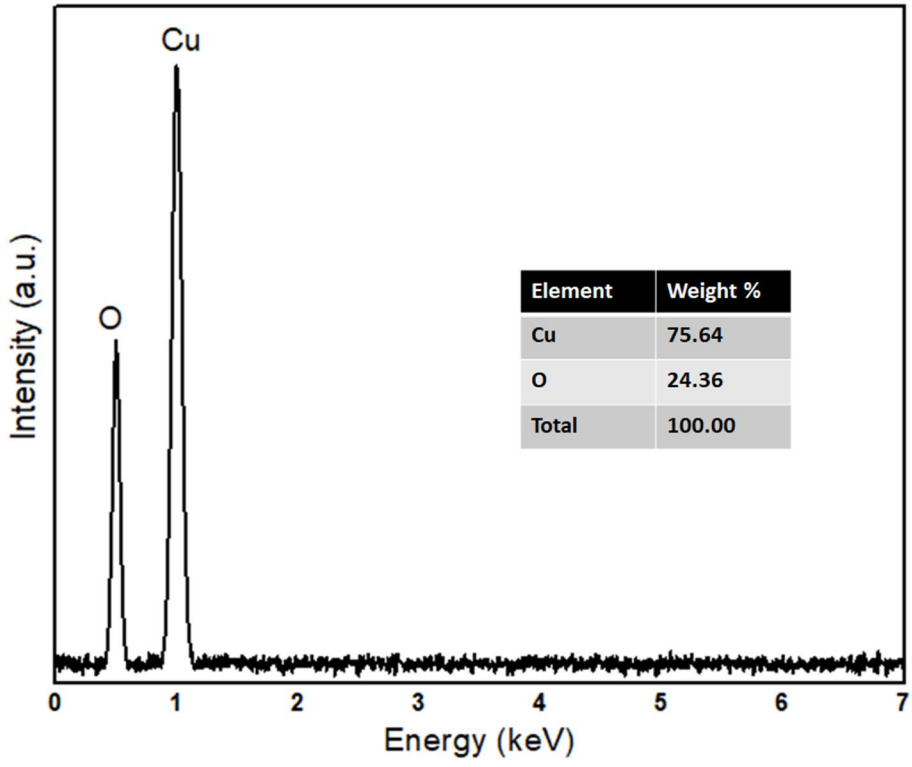

Fig. 4 Energy-dispersive X-ray spectroscopy (EDX) spectrum of SDS-stabilized CuO nanoparticles (sample 2), confirming the elemental composition. The strong peaks corresponding to copper (Cu) and oxygen (O) indicate successful synthesis of CuO with no detectable impurity elements. The quantified atomic ratio shows a Cu content of 75.64% and O content of 24.36% by weight

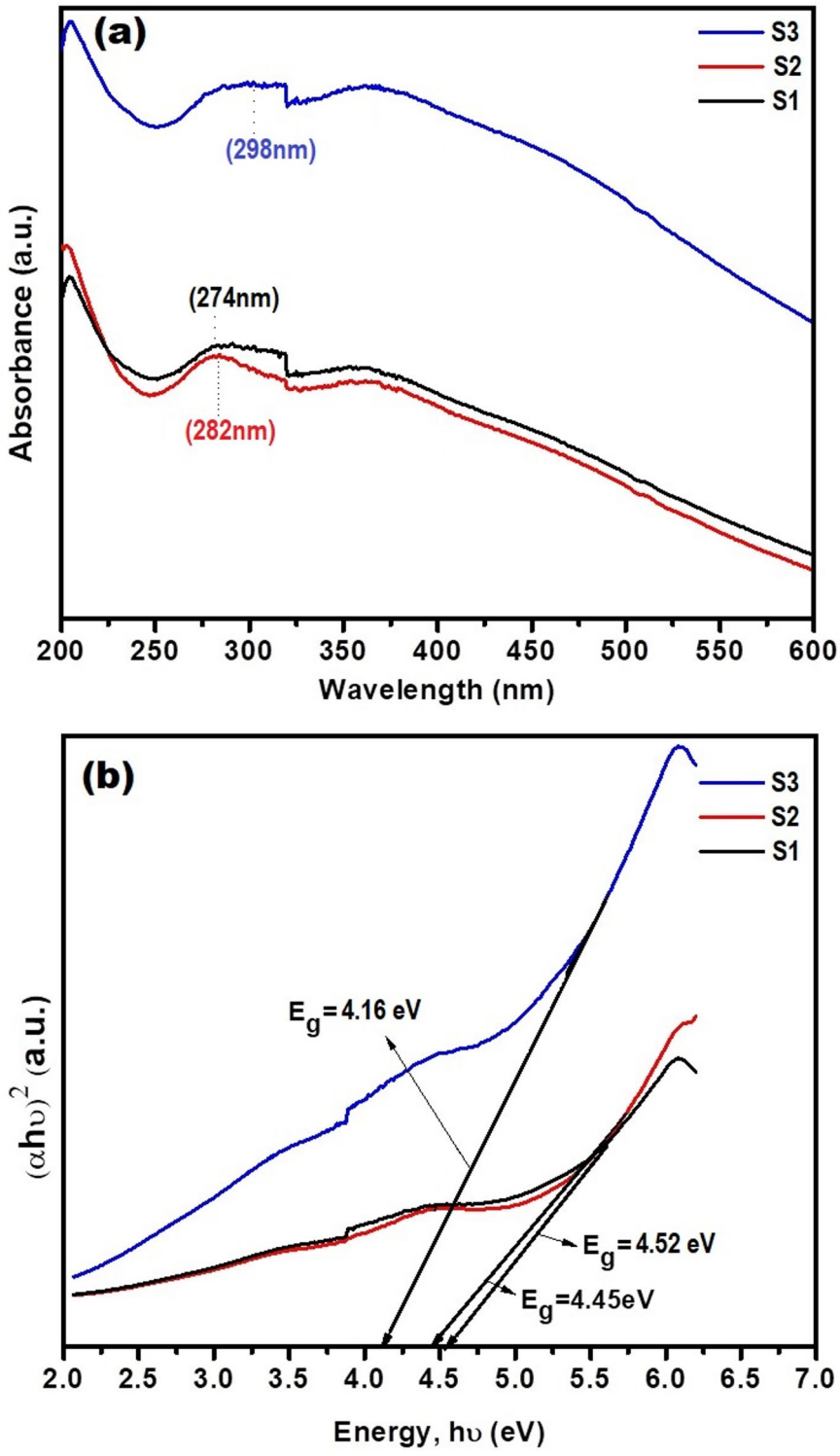

Fig. 5 UV–vis spectra and band gap estimation of SDS-stabilized CuO nanoparticles (CuO NPs). **a** UV–vis absorption spectra of SDS-stabilized CuO NPS synthesized at varying NaOH concentrations (samples S1, S2, and S3). **b** Tauc plots used to estimate the optical band gaps of the nanoparticles. The extrapolated linear regions yield band gap values of 4.52 eV (S1), 4.45 eV (S2), and 4.16 eV (S3)

band gaps were estimated using Tauc plots [50]. by extrapolating the linear regions of (αhν)2 versus hν curves (Fig. 5b). Particularly, the peak intensity in the absorption spectra decreased with increasing NaOH concentration, and a corresponding decrease in the band gap was observed. These results suggest that the optical properties of the CuO NPs are influenced by the synthesis conditions, particularly the NaOH concentration. The observed redshift in the absorption edge with increasing NaOH concentration may be attributed to an increase in nanoparticle size, as seen in SEM analysis. Additionally, changes in surface defect density and interactions between SDS and the CuO surface at higher base concentrations may also contribute to the shift in absorption behaviour.

3.5 FTIR analysis

The presence of various functional groups in the synthesized CuO NPs was investigated using FTIR. The FTIR spectra of the CuO NPs were recorded in the range of 500–4000 cm^{-1}. The spectra exhibited several characteristic peaks at 3568 cm^{-1}, 3296 cm^{-1}, 2169 cm^{-1}, 1597 cm^{-1}, 1471 cm^{-1}, 1324 cm^{-1}, 1087 cm^{-1}, 828 cm^{-1}, and 677 cm^{-1} (Fig. 6). The broad absorption bands above 3000 cm^{-1} are attributed to O–H stretching vibrations, which likely arise from adsorbed moisture or surface hydroxyl groups. While such features are commonly associated with metal hydroxides, the absence of $Cu(OH)_2$ or other secondary phases in XRD analysis confirms the formation of pure monoclinic CuO. These FTIR peaks are therefore interpreted as surface-bound features rather than evidence of incomplete conversion.

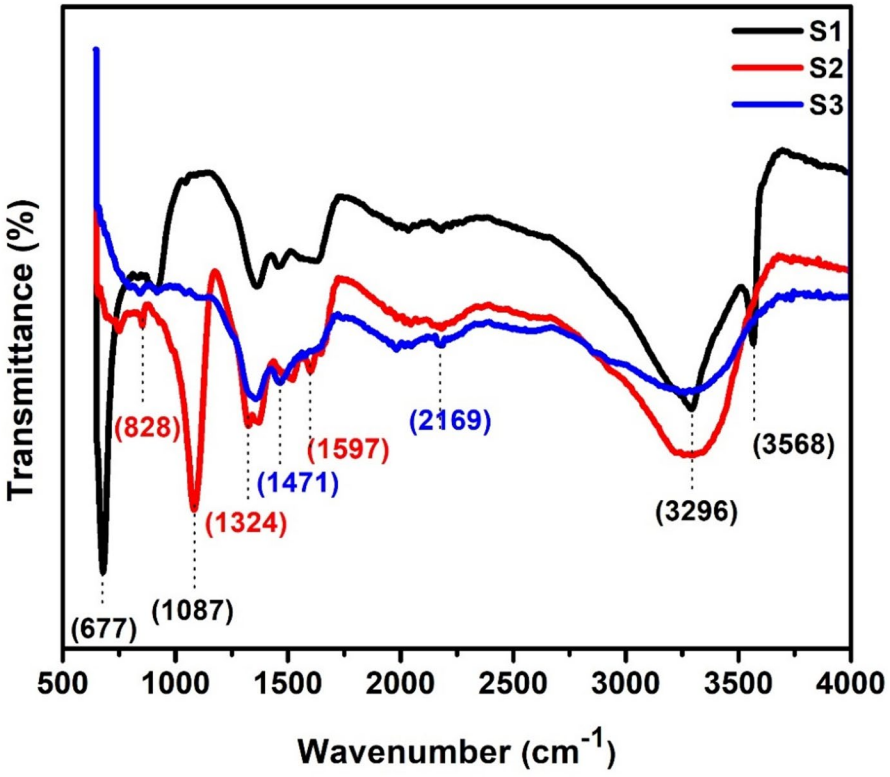

Fig. 6 FTIR spectra of SDS-coated CuO nanoparticles (CuO NPs) synthesized at varying molar ratios of precursor: surfactant: NaOH. The spectra highlight the key functional groups and provide insights into the chemical interactions between SDS and CuO, confirming the successful synthesis and stabilization of the nanoparticles

The prominent peak at 677 cm^{-1} is attributed to the Cu–O stretching vibration, confirming the formation of CuO NPs. This observation is consistent with previous FTIR studies on CuO nanostructures, which reported similar Cu–O stretching modes [51, 52]. The peaks near 1324–1597 cm^{-1} may correspond to C–H bending vibrations or symmetric stretching of–CH_2 groups introduced by SDS, while the peak at 1087 cm^{-1} is likely associated with S=O stretching of the sulphate group from SDS. These features suggest surface adsorption of SDS on the CuO NPs, supporting its role as a stabilizing agent.

3.6 Photocatalytic activity of SDS/CuO NPs

The size and shape of nanoparticles play a critical role in their photocatalytic properties. In this study, SDS/CuO NPs synthesized with a 1:1:3 molar ratio of precursor, surfactant, and base were chosen for photocatalytic experiments due to their moderate particle size and good dispersion as observed in SEM analysis. Although SEM indicated that particle size increased with NaOH concentration, the improved surface separation and higher crystallinity at this ratio likely enhanced light absorption and surface reactivity, contributing to better photocatalytic performance.

These SDS/CuO NPs were employed as photocatalysts for the degradation of MB under UV light irradiation. A 125 W UV lamp ($\lambda = 254$ nm) was used at a fixed distance of 15 cm, and the reaction was carried out under ambient temperature with continuous stirring. The initial pH of the MB solution was ~6.9 and remained near neutral throughout the experiment. Before illumination, the reaction mixtures were stirred in the dark for 30 min to achieve adsorption–desorption equilibrium. To assess the effect of dye concentration on photocatalytic efficiency, we tested three different concentrations of MB dye (20 mg/L, 30 mg/L, and 40 mg/L) using a constant photocatalyst dose of 0.5 mg/L. Furthermore, to evaluate the influence of photocatalyst dose, the degradation of 20 mg/L MB dye was investigated at various photocatalyst doses (0.1 mg/L, 0.3 mg/L, and 0.5 mg/L) (Fig. 7).

3.7 Effect of SDS/CuO NPs on photocatalytic efficiency

The influence of varying concentrations of SDS/CuO NPs on the photocatalytic efficiency was evaluated. A 20 mg/L MB solution was used, with CuO NPs added at concentrations of 0.1 mg/L, 0.3 mg/L, and 0.5 mg/L. An increase in photocatalyst concentration led to enhanced MB degradation efficiency (Fig. 8). The addition of more CuO NPs increases the available surface area for reactant adsorption, thereby providing more active sites for the photocatalytic reactions [53]. Interestingly, the highest degradation efficiency of 87% was achieved at 0.3 mg/L, beyond which the efficiency slightly declined at 0.5 mg/L. This may be attributed to excessive catalyst loading causing light scattering and reduced photon penetration, which can lower photocatalytic performance. A detailed comparison of the degradation rates and the kinetic study for different concentrations of CuO NPs demonstrates the optimal photocatalytic performance at this specific dose (Fig. 8).

3.8 Effect of dye concentration on photocatalytic degradation

The effect of varying MB dye concentrations on the photocatalytic degradation was investigated using a 0.5 mg/L dose concentration of CuO NPs (Fig. 9). MB solutions with concentrations of 20 mg/L, 30 mg/L, and 40 mg/L were tested with the fixed

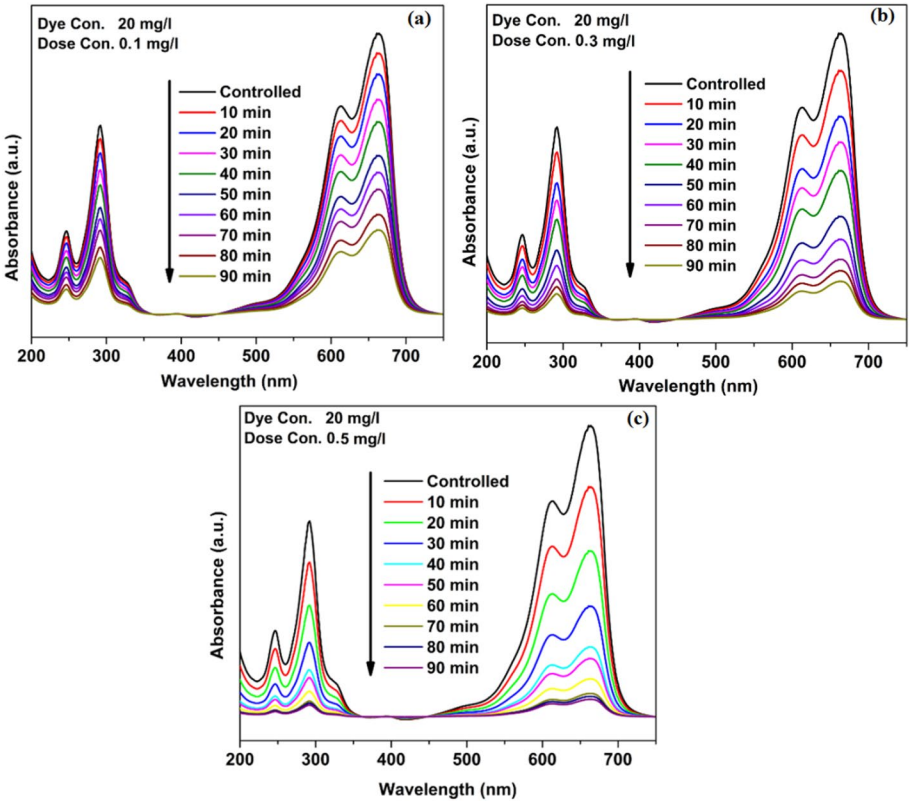

Fig. 7 Photocatalytic degradation of methylene blue (MB) dye using CuO nanoparticles (CuO NPs) at different dosages: **a** 0.1 mg/L, **b** 0.3 mg/L, and **c** 0.5 mg/L. The degradation efficiency is shown in response to varying CuO concentrations, demonstrating the influence of nanoparticle dosage on the photocatalytic activity against a fixed MB concentration of 20 mg/L

photocatalyst dose of 0.5 mg/L. The results revealed that nearly 94% degradation was achieved when the dye concentration was 20 mg/L, indicating the highest photocatalytic efficiency at this dye concentration. As the dye concentration increased, the degradation efficiency decreased. This inverse trend can be attributed to the saturation of active sites on the nanoparticle surface and reduced light penetration due to the higher optical density of the solution. Excess dye molecules may also shield the catalyst surface, limiting photon. absorption and reactive oxygen species (ROS) generation

3.9 Antifungal activity of CuO NPs

The antifungal potential of the synthesized CuO NPs was evaluated *in vitro* against *P. myriotylum* and *P. capsici*, at varying concentrations (100 ppm, 200 ppm, and 300 ppm) using the disc diffusion assay (Table 1).

For *P. myriotylum*, all CuO NPs samples exhibited concentration-dependent mycelial growth inhibition. Among the three tested samples, CuO sample-2 showed the significantly higher inhibition, with 62.3% at 300 ppm, 56.5% at 200 ppm, and 43.0% at 100 ppm. In contrast, samples 1 and 3 demonstrated lower inhibition, ranging from 26.6 to 45.9% (Table 1). Untreated PDA plates served as negative controls, and no inhibition was observed, confirming the antifungal effect of the CuO NPs.

For *P. capsici*, similar dose-dependent inhibition was observed. CuO sample-2 again showed the significantly higher efficacy with 66.4% inhibition at 300 ppm, 52.8% at 200 ppm, and 34.6% at 100 ppm, while samples 1 and 3 ranged from 25.7 to 57.5% (Table 1).

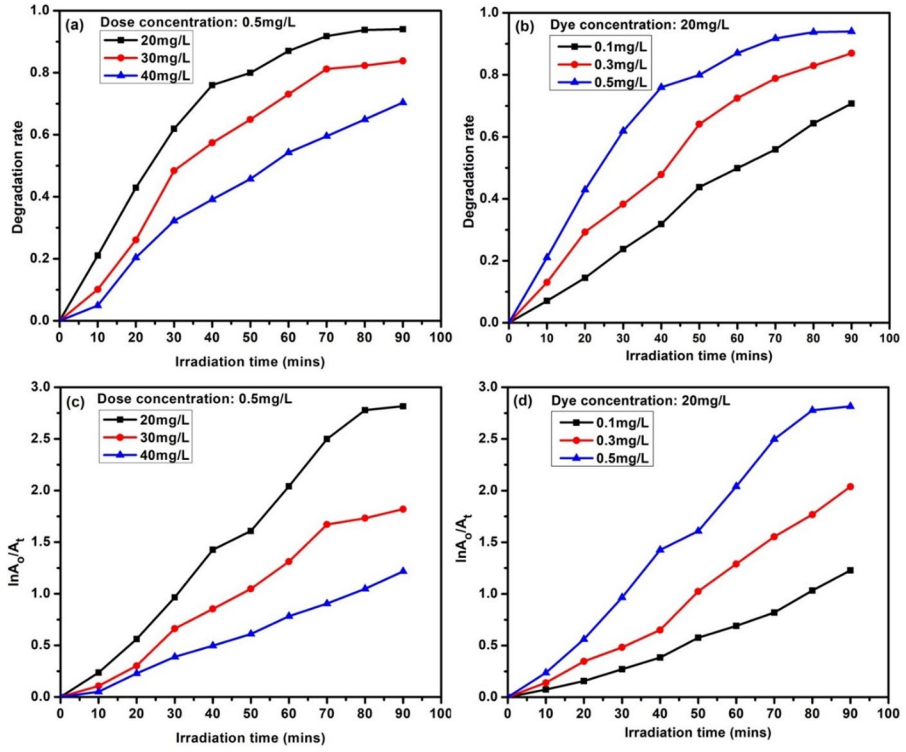

Fig. 8 Photocatalytic degradation of methylene blue (MB) dye using SDS/CuO NPs under varying conditions: **a** Effect of different dye concentrations (20 mg/L, 30 mg/L, and 40 mg/L) on degradation rate; **b** Influence of varying CuO nanoparticle (CuO NPs) dosages (0.1 mg/L, 0.3 mg/L, and 0.5 mg/L) on the degradation efficiency; **c** Kinetic study of MB degradation at different dye concentrations; **d** Kinetic analysis of the degradation process at varying CuO NPs dosages

The enhanced performance of sample-2 may be attributed to its optimal balance of particle size, surface stabilization by SDS, and crystallinity, as indicated by SEM and XRD analyses.

4 Discussion

The successful synthesis of SDS-stabilized CuO NPs using varying NaOH concentrations was confirmed through structural and morphological analyses. Key parameters such as crystallinity, particle size, and dispersion appeared to be influenced by NaOH concentration and SDS stabilization. These findings suggest a relationship between synthesis conditions and nanoparticle quality, which forms the basis for evaluating their photocatalytic and antifungal performance.

NaOH concentration seemed to play a critical role in affecting nanoparticle morphology and aggregation. At lower NaOH concentrations (e.g., 1.34 g), fewer CuO NPs were observed, and SEM images showed significant agglomeration, possibly due to stronger interparticle forces. This may result from rapid diffusion of Cu^{2+} and OH^- ions onto the crystal surface, potentially leading to uncontrolled nucleation. In contrast, higher NaOH concentrations (4.02 g and 6.7 g) led to more uniform and larger particles with reduced agglomeration. This trend may be related to slower nucleation and more controlled growth, although no *in situ* or kinetic measurements were conducted.

The spherical morphology observed at all concentrations was further enhanced by the capping effect of SDS, which stabilized the particles and prevented aggregation. This

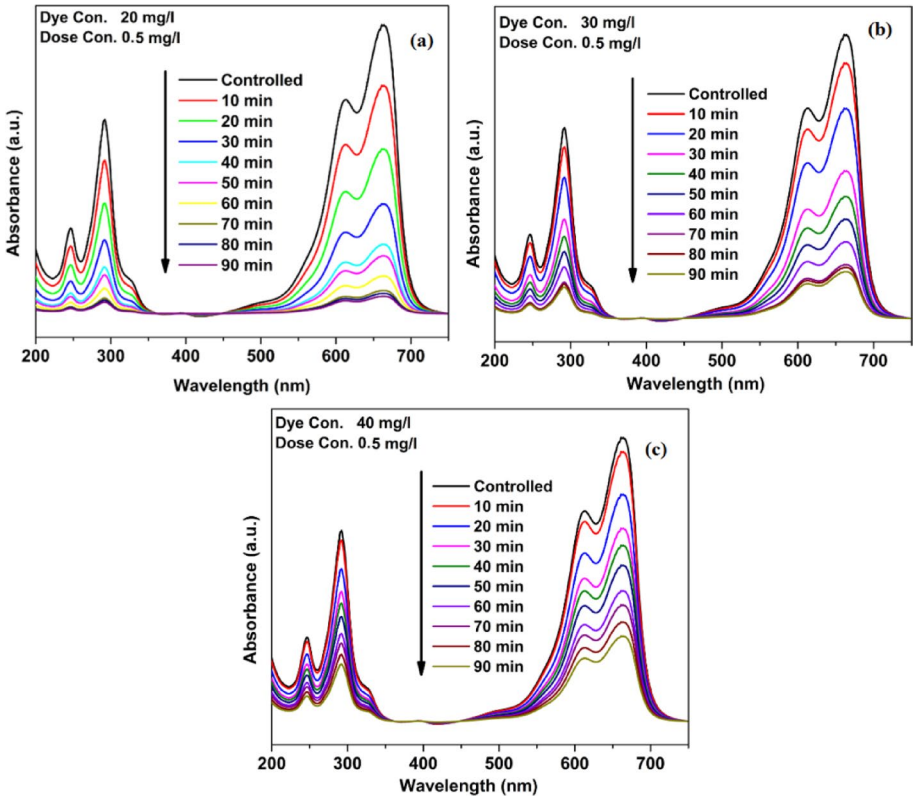

Fig. 9 Photocatalytic degradation of methylene blue (MB) using SDS/CuO NPs with a CuO dosage of 0.5 mg/L at varying MB concentrations: **a** 20 mg/L, **b** 30 mg/L, and **c** 40 mg/L

Table 1 Antifungal activity of SDS-mediated CuO nanoparticles against *Pythium myriotylum* and *Phytophthora capsici*, shown as mean inhibition zone diameters (cm) ± SE at various nanoparticle concentrations

Treatment	*Pythium myriotylum*		*Phytophthora capsici*	
	Mean (cm) ± SE	*GI	Mean (cm) ± SE	*GI
CuO sam-1 (100 ppm)	4.57 ± 0.20 bc	33.8%	5.30 ± 0.15 b	25.7%
CuO sam-1 (200 ppm)	4.37 ± 0.22 cd	36.7%	3.83 ± 0.15 ef	46.3%
CuO sam-1 (300 ppm)	3.83 ± 0.19 e	44.4%	3.03 ± 0.23 g	57.5%
CuO sam-2 (100 ppm)	3.93 ± 0.18 e	43.0%	4.67 ± 0.15 cd	34.6%
CuO sam-2 (200 ppm)	3.00 ± 0.15 f	56.5%	3.37 ± 0.17 fg	52.8%
CuO sam-2 (300 ppm)	2.60 ± 0.17 f	62.3%	4.20 ± 0.12 de	66.4%
CuO sam-3 (100 ppm)	5.07 ± 0.19 b	26.6%	4.97 ± 0.20 bc	30.4%
CuO sam-3 (200 ppm)	4.53 ± 0.18 c	34.3%	3.47 ± 0.27 fg	51.4%
CuO sam-3 (300 ppm)	3.73 ± 0.15 e	45.9%	3.30 ± 0.21 fg	53.7%
Control	6.90 ± 0.21 a	0.00%	7.13 ± 0.35 a	0.0

Different letters indicate statistically significant differences between samples as determined by fisher's least significant difference (LSD)

*GI: Growth inhibition

stabilization is likely due to the electrostatic repulsion introduced by the anionic sulphate head groups of SDS adsorbing onto the nanoparticle surface. Beyond preventing aggregation, SDS may also influence the surface charge of the nanoparticles, potentially enhancing their dispersion in aqueous media [36]. This surface modification could affect interactions with fungal cell membranes or dye molecules by altering hydrophobicity and surface reactivity [54, 55]. However, no direct confirmation of SDS binding such

as FTIR peak shifts, zeta potential measurements, or surface energy analysis was performed. Therefore, whether SDS acts solely through electrostatic stabilization, or also functions as a micelle template or surface ligand, remains uncertain. Although surface charge and Cu^{2+} ion release was not measured here, both factors may contribute to the observed antifungal and photocatalytic activity and warrant further investigation.

UV–vis absorption spectra revealed a redshift in optical transitions with increasing NaOH concentrations, consistent with the observed decrease in band gap energy (from 4.52 to 4.16 eV). This trend likely reflects changes in electronic structure associated with increased nanoparticle size and surface modifications induced by SDS stabilization. Although the band gaps are significantly higher than those of bulk CuO (~ 1.2 to 1.9 eV), this may result from combined effects of nanoscale size, SDS interactions, and the use of a direct transition model in Tauc analysis. While quantum confinement may contribute, further validation using photoluminescence spectroscopy or band structure modeling is required. FTIR spectra confirmed the presence of O–H groups, C–N stretching, and C–O vibrations associated with flavonoids, providing insight into the surface chemistry of the synthesized nanoparticles and further indicating the impact of NaOH on NP composition and surface functionalization [51, 56–58].

The formation mechanism involved co-precipitation of $Cu(OH)_2$ from a mixture of copper chloride ($CuCl_2$), copper nitrate ($Cu(NO_2)_2$), and NaOH, followed by thermal decomposition into CuO. Trace formation of Cu_2O was attributed to the partial reduction of CuO under certain conditions, especially in the presence of excess Cu, which favours the formation of thermodynamically stable Cu(I) oxide in the solid state [41, 59]. SDS not only stabilized the particles during this transformation but also influenced surface properties that likely enhanced the observed functionalities [36].

The photocatalytic performance of SDS-CuO NPs was evaluated by their ability to degrade MB dye under UV irradiation. Upon light exposure, the CuO NPs absorb energy and generate electron–hole pairs, which initiate a cascade of redox reactions. Photogenerated holes can oxidize adsorbed water molecules to produce hydroxyl radicals (·OH), while conduction band electrons may reduce molecular oxygen to form superoxide radicals (O_2–), both of which are ROS that contribute to dye degradation. Increased CuO dosage enhanced the photocatalytic activity due to the availability of more surface-active sites, and improved particle dispersion with degradation following pseudo-first-order kinetics, confirming high catalytic efficiency [53, 60, 61]. This is consistent with recent reports demonstrating the photocatalytic efficacy of CuO-based nanomaterials in dye degradation systems under UV and visible light [62, 63]. A similar study also demonstrated the catalytic degradation of MB using Cu-based nanostructures, further supporting the effectiveness of such materials for dye removal applications [64].

The antifungal efficacy of the CuO NPs was also significant. Their nanoscale size enabled close interaction with fungal cell walls, facilitating penetration and intracellular generation of ROS, including ·OH, O_2–, and H_2O_2. These reactive species are believed to induce oxidative stress by disrupting fungal membrane integrity, damaging intracellular organelles, and impairing metabolic function. These ROS caused oxidative stress, damaging cellular membranes and components, ultimately inhibiting fungal growth [54, 55, 58, 65]. Among all synthesized samples, CuO sample-2 exhibited the strongest antifungal activity, with mycelial growth inhibition ranging from 43.0 to 62.3% for *P. myriotylum* and 34.6–66.4% for *P. capsici*. This enhanced activity may be attributed to its

intermediate particle size and improved dispersion, as observed in SEM analysis. Compared to the smaller but more agglomerated sample-1 and the larger sample-3, sample-2 likely presented an optimal surface area-to-particle contact ratio, enabling more effective interaction with fungal cells and ROS-mediated damage. Additional factors such as localized Cu^{2+} ion release, alteration of fungal redox signalling, or modulation of membrane permeability may also contribute to the antifungal mechanism. These results surpassed the inhibitory rates reported by Banik and Pérez-de-Luque, who achieved 60% inhibition of *Phytophthora cinnamomi* at 100 mg/L CuO NP concentration [32, 66]. Our findings support recent studies emphasizing the broad-spectrum antifungal potential of CuO NPs against plant pathogens [28, 31]. Additional recent reports also highlight the antifungal and antimicrobial potential of metal oxide nanostructures in agricultural contexts [67, 68].

5 Conclusions

This study demonstrates that SDS-stabilized CuO NPs synthesized via a chemical precipitation method exhibit measurable antifungal and photocatalytic activity under controlled laboratory conditions. Among the three formulations tested, the nanoparticles synthesized at a 1:1:3 molar ratio of precursor, surfactant, and NaOH showed the most effective performance. These nanoparticles achieved up to 94% degradation of methylene blue under UV light and a maximum mycelial growth inhibition of 62.3% and 66.4% against *P. myriotylum* and *P. capsica* respectively. These findings reflect, *in vitro* performance, and do not yet confirm practical applicability in field or environmental systems. The antifungal and photocatalytic activities were evaluated independently. Future research should focus on validating the underlying mechanisms (e.g., ROS detection), testing reusability and long-term nanoparticle stability, and performing comparative studies with conventional fungicides and photocatalysts. Additional work should also assess Cu^{2+} leaching, phytotoxicity, and interactions with soil and microbial ecosystems. Field trials and environmental risk assessments will be essential to determine the safety, efficacy, and scalability of SDS-CuO NPs for agricultural or wastewater treatment applications.

Acknowledgements
Authors would like to express sincere gratitude to the Department of Plant Protection Biology, Swedish University of Agricultural Sciences, Sweden for providing the necessary resources and support throughout the research.

Author contributions
Conceptualization: BSK, MI and MB; methodology: IR, SH, and NA; software: SSH, and AS; validation: AS and BSK; formal analysis: BSK, I, BS and MB; investigation: IR, SH and NA; resources; BSK, MI, and MB; data curation: ZFR and BSH; writing—original draft preparation: IR, SH, BSK, NA, I, BSH; writing—review and editing: MI; visualization: BSK; supervision: BSK, MI and MB; project administration: BSK and MB. All authors have read and agreed to the published version of the manuscript.

Funding
Open access funding provided by Swedish University of Agricultural Sciences. This research was supported by the institutions involved in the study.

Data availability
All data generated or analysed during this study are included in this published article.

Declarations

Ethics approval and consent to participate
Not applicable.

Consent for publication
Not applicable.

Clinical trial number
Not applicable.

Competing interests
The authors declare no competing interests.

Received: 14 April 2025 / Accepted: 21 July 2025
Published online: 28 July 2025

References

1. Tariq M, et al. Yield potential study of *Capsicumannuum* L. under the application of PGPR. Adv Life Sci. 2014;1:202–7.
2. Jayapala N, et al. Rhizobacteria *Bacillus* spp. induce resistance against anthracnose disease in chili (*Capsicumannuum* L.) through activating host defense response. Egypt J Biol Pest Control. 2019;29:1–9.
3. Hyder S, et al. Characterization of native plant growth promoting rhizobacteria and their anti-oomycete potential against *Phytophthoracapsici* affecting chilli pepper (*Capsicumannuum* L.). Sci Rep. 2020;10:1–15.
4. Hyder S, et al. Biological control of chili damping-off disease, caused by *Pythiummyriotylum*. Front Microbiol. 2021;12: 587431.
5. Sanogo S, Ji P. Integrated management of *Phytophthoracapsici* on solanaceous and cucurbitaceous crops: current status, gaps in knowledge and research needs. Can J Plant Pathol. 2012;34:479–92.
6. Cuervo-Parra J, et al. Morphological and molecular characterization of *Moniliophthororareri*, causal agent of frosty pod rot of cocoa tree in Tabasco. Mexico Plant Pathol J. 2011;10:122–7.
7. Iqbal M, et al. Evaluation of *Clonostachysrosea* for control of plant-parasitic nematodes in soil and in roots of carrot and wheat. Phytopathology. 2018;108:52–9.
8. Iqbal M, et al. Biological control of strawberry crown rot, root rot and grey mould by the beneficial fungus *Aureobasidiumpullulans*. Biocontrol. 2021;66:535–45.
9. Krauss U, et al. Mycoparasitism by *Clonostachysbyssicola* and *Clonostachysrosea* on *Trichoderma* spp. from cocoa (*Theobromacacao*) and implication for the design of mixed biocontrol agents. Biol Control. 2013;67:317–27.
10. Mbarga JB, et al. A new oil-based formulation of *Trichodermaasperellum* for the biological control of cacao black pod disease caused by *Phytophthoramegakarya*. Biol Control. 2014;77:15–22.
11. Iqbal M, et al. Bee-vectored *Aureobasidiumpullulans* for biological control of gray mold in strawberry. Phytopathology. 2022;112:232–7.
12. Iqbal M, et al. Biocontrol potential of beneficial fungus *Aureobasidiumpullulans* against *Botrytiscinerea* and *Colletotrichumacutatum*. Phytopathology. 2023;113:1428–38.
13. Oladoye PO, et al. Methylene blue dye: toxicity and potential elimination technology from wastewater. Results Eng. 2022;16: 100678.
14. Kubra KT, Salman MS, Hasan MN. Enhanced toxic dye removal from wastewater using biodegradable polymeric natural adsorbent. J Mol Liq. 2021;328: 115468.
15. Diem PNH, et al. Silver, gold, and silver–gold bimetallic nanoparticle-decorated dextran: facile synthesis and versatile tunability on the antimicrobial activity. J Nanomater. 2020;2020:1–11.
16. Wang L, Hu C, Shao L. The antimicrobial activity of nanoparticles: present situation and prospects for the future. Int J Nanomed. 2017;12:1227.
17. Soltani Nezhad S, et al. Isolation of copper oxide (CuO) nanoparticles resistant *Pseudomonas* strains from soil and investigation on possible mechanism for resistance. World J Microbiol Biotechnol. 2014;30:809–17.
18. Khan BS, et al. Mechanism for the formation of cuprous oxide nanowires in AAO template by electrodeposition. Int J Electrochem Sci. 2017;12:890–7.
19. Sivaraj R, et al. Biosynthesis and characterization of *Acalypha indica*-mediated copper oxide nanoparticles and evaluation of its antimicrobial and anticancer activity. Spectrochim Acta A Mol Biomol Spectrosc. 2014;129:255–8.
20. Omran BA, et al. Myco-architecture of proficient antibacterial CuO/Ag_2O-grafted graphene oxide nanoconjugates: characterization and Congo red degradation-assisted by the activation of peroxymonosulfate. Mater Res Bull. 2025;190: 113496.
21. Thakur S, et al. Growth mechanism and characterization of CuO nanostructure as a potent antimicrobial agent. Surf Interfaces. 2020;20: 100551.
22. Omran BA, et al. Synthesis of TiO_2–CuO@graphene oxide hybrid bionanocomposite with enhanced antibacterial and organic dye degradation activities. Mater Adv. 2025;6:2654–76.
23. Omran BA, et al. Biogenically synthesized copper oxide, titanium oxide, and silver oxide nanoparticles: characterization and biological effects. Clean Technol Environ Policy. 2024;26:1–26.
24. Omran BA, et al. Mycofabrication of bimetal oxide nanoparticles (CuO/TiO_2) using the endophytic fungus *Trichodermavirens*: material properties and microbiocidal effects against bacterial pathogens. Ceram Int. 2024;50:30843–57.
25. Chen X, et al. Shape-induced ultraviolet absorption of CuO shuttlelike nanoparticles. Appl Phys Lett. 2007;90: 183118.
26. Azam A, et al. Size-dependent antimicrobial properties of CuO nanoparticles against Gram-positive and -negative bacterial strains. Int J Nanomed. 2012;7:3527–35.
27. Neupane MP, et al. Temperature driven morphological changes of hydrothermally prepared copper oxide nanoparticles. Surf Interface Anal. 2009;41:259–63.
28. Sawake MM, et al. Management of *Phytophthoraparasitica* causing gummosis in citrus using biogenic copper oxide nanoparticles. J Appl Microbiol. 2022;132:3142–54.
29. Zhu J, et al. Highly dispersed CuO nanoparticles prepared by a novel quick-precipitation method. Mater Lett. 2004;58:3324–7.
30. Kayani ZN, et al. Characterization of copper oxide nanoparticles fabricated by the sol–gel method. J Electron Mater. 2015;44:3704–9.
31. El-Batal AI, et al. *Penicilliumchrysogenum*-mediated mycogenic synthesis of copper oxide nanoparticles using gamma rays for in vitro antimicrobial activity against some plant pathogens. J Clust Sci. 2020;31:79–90.

32. Thakur S, et al. Green synthesis of copper nanoparticles using *Asparagusadscendens* Roxb. root and leaf extract and their antimicrobial activities. Int J Curr Microbiol Appl Sci. 2018;7:683–94.
33. Kamel SM, et al. Antifungal activity of copper oxide nanoparticles against root rot disease in cucumber. J Fungi. 2022;8:911.
34. Shah J, et al. Surfactant prevented growth and enhanced thermos physical properties of CuO nanofluid. J Mol Liq. 2019;283:550–7.
35. Shahmiri M, et al. Preparation of PVP-coated copper oxide nanosheets as antibacterial and antifungal agents. J Mater Res. 2013;28:3109–18.
36. Ganga B, Santhosh P. Manipulating aggregation of CuO nanoparticles: correlation between morphology and optical properties. J Alloys Compd. 2014;612:456–64.
37. Reddy S, Swamy BK, Jayadevappa H. CuO nanoparticle sensor for the electrochemical determination of dopamine. Electrochim Acta. 2012;61:78–86.
38. Namburu PK, et al. Viscosity of copper oxide nanoparticles dispersed in ethylene glycol and water mixture. Exp Therm Fluid Sci. 2007;32:397–402.
39. Qiang AH, et al. Effect of dispersant on the colloidal stability of nano-sized CuO suspension. J Dispers Sci Technol. 2007;28:1004–7.
40. Rao MP, et al. Surfactant assisted synthesis of copper oxide nanoparticles for photocatalytic degradation of methylene blue in the presence of visible light. Energy Environ Focus. 2015;4:250–5.
41. Chen D, et al. Preparation of Cu_2O nanoparticles in cupric chloride solutions with a simple mechanochemical approach. J Alloys Compd. 2010;504:S345–8.
42. Niraula TP, et al. Sodium dodecylsulphate: a very useful surfactant for scientific investigations. J Knowl Innov. 2014;2:111–3.
43. Piret J, Désormeaux A, Bergeron MG. Sodium lauryl sulfate, a microbicide effective against enveloped and nonenveloped viruses. Curr Drug Targets. 2002;3:17–30.
44. Parekh ZR, et al. CuO nanoparticles—synthesis by wet precipitation technique and its characterization. Phys B Condens Matter. 2021;610: 412950.
45. Vijayaraghavan T, et al. Rapid and efficient visible light photocatalytic dye degradation using AFe_2O_4 (A = Ba, Ca and Sr) complex oxides. Mater Sci Eng B. 2016;210:43–50.
46. Hyder S, et al. First report of *Pythiummyriotylum* causing damping off and root rot in chili pepper (*Capsicumannuum* L.) from Punjab Pakistan. Plant Dis. 2018;102:687.
47. Jeyarani WJ, et al. An investigation on the tuning effect of glucose-capping on the size and bandgap of CuO nanoparticles. Adv Powder Technol. 2016;27:338–46.
48. Taghavi Fardood S, Ramazani A. Green synthesis and characterization of copper oxide nanoparticles using coffee powder extract. J Nanostruct. 2016;6:167–71.
49. Giahi M, et al. Synthesis of CuO/ZnO nanoparticles and their application for photocatalytic degradation of lidocaine HCl by the trial-and-error and Taguchi methods. Bull Korean Chem Soc. 2013;34:2176–82.
50. Viezbicke BD, et al. Evaluation of the Tauc method for optical absorption edge determination: ZnO thin films as a model system. Phys Status Solidi B. 2015;252:1700–10.
51. Andualem WW, et al. Synthesis of copper oxide nanoparticles using plant leaf extract of *Cathaedulis* and its antibacterial activity. J Nanotechnol. 2020;2020:1–10.
52. Alhalili Z. Green synthesis of copper oxide nanoparticles CuO NPs from *Eucalyptusglobulus* leaf extract: adsorption and design of experiments. Arab J Chem. 2022;15: 103739.
53. Dulta K, et al. Multifunctional CuO nanoparticles with enhanced photocatalytic dye degradation and antibacterial activity. Sustain Environ Res. 2022;32:1–15.
54. Parveen S, et al. Preparation, characterization and antifungal activity of iron oxide nanoparticles. Microb Pathog. 2018;115:287–92.
55. Applerot G, et al. Understanding the antibacterial mechanism of CuO nanoparticles: revealing the route of induced oxidative stress. Small. 2012;8:3326–37.
56. Tahir A, et al. Mechanism for the formation of magnetite iron oxide nanostructures by *Ficuscarica* dried fruit extract using green synthesis method. Appl Nanosci. 2021;11:1857–65.
57. Atri A, et al. Green synthesis of copper oxide nanoparticles using *Ephedraalata* plant extract and a study of their antifungal, antibacterial activity and photocatalytic performance under sunlight. Heliyon. 2023;9:e13484.
58. Mazhar S, et al. Green synthesis of silver nanoparticles using guava leaves: an effective strategy to control chilli fruit rot disease. BMC Plant Biol. 2025;25:499.
59. Zhao H, et al. Fabrication of a palladium nanoparticle/graphene nanosheet hybrid via sacrifice of a copper template and its application in catalytic oxidation of formic acid. Chem Commun. 2011;47:2014–6.
60. Zeng JH, Jin BB, Wang YF. Facet enhanced photocatalytic effect with uniform single-crystalline zinc oxide nanodisks. Chem Phys Lett. 2009;472:90–5.
61. Katwal R, et al. Electrochemical synthesized copper oxide nanoparticles for enhanced photocatalytic and antimicrobial activity. J Ind Eng Chem. 2015;31:173–84.
62. Priyadharsan A, et al. Effect of metal doping and non-metal loading on light energy driven degradation of organic dye using ZnO nanocatalysts. Chemosphere. 2023;330: 138708.
63. Liu H, et al. Photocatalytic activity study of ZnO modified with nitrogen–sulfur co-doped carbon quantum dots under visible light. New J Chem. 2022;46:14867–78.
64. Anjum SM, Riazunnisa K. Fine ultra-small ruthenium oxide nanoparticle synthesis by using *Catharanthusroseus* and *Moringaoleifera* leaf extracts and their efficacy towards in vitro assays, antimicrobial activity and catalytic: adsorption kinetic studies using methylene blue dye. J Clust Sci. 2022;33:1103–17.
65. Wang J-W, et al. Regulating the regulators: microRNA and asthma. World Allergy Organ J. 2011;4:94–103.
66. Banik S, Pérez-de-Luque A. In vitro effects of copper nanoparticles on plant pathogens, beneficial microbes and crop plants. Span J Agric Res. 2017;15: e1005.
67. Kamaraj C, et al. Sustainable development through the bio-fabrication of ecofriendly ZnO nanoparticles and its approaches to toxicology and environmental protection. Biomass Convers Biorefin. 2024;14:28533–49.

68. Ragavendran C, et al. Green-route synthesis of ZnO nanoparticles via *Solanumsurattense* leaf extract: characterization, biomedical applications and their ecotoxicity assessment of zebrafish embryo model. S Afr J Bot. 2024;167:643–62.

Publisher's note